

Lighting the Landscape: Molecular Events Under Dynamic Stark Shifts

Bo Y. Chang,¹ Ignacio R. Sola,² and Seokmin Shin¹

¹*School of Chemistry (BK21), Seoul National University, Seoul 151-747, Republic of Korea*

²*Departamento de Química Física, Universidad Complutense, 28040 Madrid, Spain**

A new perspective on how to manipulate molecules by means of very strong laser pulses is emerging with insights from the so-called light-induced potentials, which are the adiabatic potential energy surfaces of molecules severely distorted by the effect of the strong field. Different effects appear depending on how the laser frequency is tuned, to a certain electronic transition, creating light-induced avoided crossings, or very off-resonant, generating Stark shifts. In the former case it is possible to induce dramatic changes in the geometry and redistribution of charges in the molecule while the lasers are acting and to fully control photodissociation reactions as well as other photochemical processes. Several theoretical proposals taken from the work of the authors are reviewed and analyzed showing the unique features that the strong-laser chemistry opens to control the transient properties and the dynamics of molecules.

INTRODUCTION

In the last few years, many techniques were developed to manipulate and control molecular processes by means of ultrashort laser pulses[1–5]. Initially, ultrashort pulses were used because they provided the means to act on the time-scale of fast molecular events[6]. At a later stage, it was the broad pulse spectrum of the pulses that by phase modulation and learning algorithms, opened great opportunities to control the dynamics[7]. More recently, the non-resonant strong-field interaction of the pulse provided a means to alter the potential energy surface of the molecule via dynamic Stark effect, "catalyzing" many photochemical processes[8–11]. While all the previous roles remain useful for different purposes, one can arguably follow this sequence of events as one in which the laser is promoted from the role of a non-specific exciter (and probe of the chemical process), to a reactant and then to a catalyst, using the chemical terminology. In this review we will outline some of our contributions in the control of molecules in the strong-field regime from a theoretical perspective. For a broader perspective the interested reader is referred to the following work and references therein[12–14].

The application of strong pulses to atoms has a long history[15–25]. Here we are interested in non-ionizing effects, which require the use of moderately-strong pulses, typically within tens of TW/cm². Thomas George and Andre Bandrauk developed a very useful "chemical" picture of light-induced events[26, 27]. In this picture, the slow effects of the field on the nuclei (averaged over the radiation cycles) are incorporated in the "dressed" (energy shifted) molecular potentials. Then, in the adiabatic representation, the dynamics of photodissociation or multiphoton processes are recast in terms of predissociation, avoided crossings, or other topological features. The adiabatic potentials that incorporate these laser-molecule coupling effects are called light-induced potentials[28] (LIPs), while the avoided crossings in the LIPs are called light-induced avoided crossings[29, 30]

(LIACs). In polyatomic molecules, or taking into account the vectorial nature of the coupling, the LIACs can be seen as light-induced conical intersections[31–39] (LICIs). Considerable theoretical effort has been put recently at characterizing the LICIs.

One of the first and most obvious applications of strong pulses is to enhance the yield of electronic absorption. However, because Raman transitions can compete with absorption and the Stark effect can decouple the electronic states, strong and ultrashort transformed-limited pulses do not lead to efficient population transfer[40–43]. One needs to resort to adiabatic rapid passage (ARP) by means of chirped pulses, or to schemes that use more than one pulse[44–48]. Simple theoretical models, such as the Landau-Zener model, were often used to explain the high yields of electronic excitation in ARP[49]. On the other hand, several schemes for population transfer with sequences of strong pulses could be designed as strong-field analogs in electronic potentials of adiabatic passage between quantum levels[50]. Adiabatic passage by light-induced potentials[51–58] (APLIP), chirped adiabatic rapid passage[59–61] (CARP), selective population of dressed states[62–65] (SPODS), rapid vibrational inversion via time-gating[29] or Raman chirped adiabatic passage[66–71] (RCAP) serve as examples.

The LIPs are not only useful as a convenient explanatory device to understand the remarkable features of population transfer under strong pulses (e.g., its robustness); they truly are potential energy surfaces that determine, for instance, the geometrical features of the molecule and their related properties. Particularly interesting are LIPs formed by coupling a bound and a dissociative molecular potential. The effect of a strong field is to mix their electronic character. The first evidence of these properties was found out after observing bond softening in the ground electronic state[72–77] and bond hardening in a dissociative potential[78–82]. Varying the intensity and frequency of the dressing field one can efficiently control the geometry of the "previously-dissociating" potential.

However, in order to change the molecular properties,

it is necessary to adiabatically prepare the system on this potential. One can then externally control the bond distance of a diatomic molecule over a very large range of values, as in the laser adiabatic manipulation of the bond (LAMB) scheme. Several two-pulse schemes and single pulses with modulated frequencies were proposed for this purpose[83–90]. If the preparation is not fully adiabatic, one can still control the transition to create oscillating nuclear wave packets of different amplitudes in the LIP, that is, to create molecular analogs of "classical-like" coherent vibrations[88, 90]. It is also possible to correct the non-adiabaticity by absorbing the excess of vibrational energy as a zero-energy of a modified LIP, via time-asymmetric pulses[91]. In addition to controlling the molecular geometry, other LIPs can be prepared to change the width of the nuclear wave packet, achieving molecular squeezing either adiabatically or dynamically[92–96]. The adiabatic methods in principle can be used to create *artificial* bond lengths and vibrations with parameters that are fully externally controlled by the laser. However, these properties are *transient*. They only exist as long as the laser is acting and no strong measurement is performed on the system.

In correspondence to the geometrical changes induced by the LIP, there are changes in the electronic properties associated to the electronic superposition state[97–100]. These properties, for example the permanent or transition dipole, reflect the underlying changes in the redistribution of charges. It was recently shown that some superpositions manifested a clear classical picture of an electron oscillating between the protons, whereas in a dressed electronic state the electron was moving along with the proton[99].

The electronic character of the LIP plays important roles in other processes as well. For instance, in the control of the spin state of the molecule, we have shown how electric pulses or electromagnetic fields can be used to avoid a singlet-triplet transition, by suitably modifying the singlet and triplet LIPs such that there is no crossing between them[101–103]. However, under usual circumstances very strong fields are needed, such that the rate of ionization at the required laser intensity is faster than the rate of inter-system conversion[104, 105]. Under certain conditions, the schemes can only operate when the spin-orbit coupling is weak, reverting to a few-level problem[105, 106].

Other intramolecular or non-adiabatic couplings can be controlled in a similar manner. For instance, one can generate LIACs that prevent the initial nuclear wave packet to reach a certain conical intersection in order to avoid energy deactivation[30]. However, most works have been done to create the LIAC or LICI in order to

control the output of a photochemical process. In particular, there have been several theoretical proposals to control the yield of a photodissociation reaction[110], as well as the branching ratio over possible fragmentation channels[35, 107, 109, 110] and the kinetic energy distribution of the fragments[111]. Although most proposals remain experimentally untested, owing to the difficulty of finding good molecular systems where the strong field interaction is strong enough to generate LIPs, yet not too strong that the ionization is predominant, recent experiments have shown that indeed such control is possible[8–10].

In this work we will review some of our findings. In Sec. 2 we will provide a simplified analysis of the geometrical and dynamical features of LIPs, outlining the role of the Stark-shift and of laser-induced potential energy shaping in several control scenarios. In Sec. 3 we present several works of our group for the control of the bond length in diatomic molecules, by using LIPs that imply contributions of bound and dissociative electronic states. In Sec. 4 we analyze the electronic character of the LIPs and the interesting views that it provides to control electronic properties such as the dipole moment. In Sec. 5 we show how one can control different observables of photodissociation reactions, such as the photodissociation spectrum, the branching ratios and the kinetic energy distribution of the fragments, by using strong nonresonant fields that couple two dissociating electronic states. Finally, Sec. 6 provides some of the relevant Conclusions.

LIGHT-INDUCED POTENTIALS: GEOMETRICAL AND DYNAMICAL FEATURES

The goal of this section is to set the stage where all the subsequent control schemes reviewed in this article operate, clarifying the relation between certain topological features of the LIPs and the quantum processes that they convey. To simplify the analysis we start by considering diatomic molecules oriented with respect to a single external field $E(t)$. We use the rotating wave approximation (RWA), such that $E(t) \approx \epsilon(t)e^{\pm i\varphi(t)}/2$, where $\epsilon(t)$ is a slowly varying envelope function, compared to the rate of change of the dynamical phase $\varphi(t)$. The negative sign is used to describe absorption, while the positive sign is used for the stimulated emission. In general, for chirped pulses, $\varphi(t) = \int \omega(t')dt'$ where $\omega(t)$ is the time-varying frequency. If we assume that only two electronic states participate in the dynamics, the following very general effective Hamiltonian can be used to describe the evolution of the nuclear wave functions in each electronic state,

$$\mathbf{H} = \begin{pmatrix} \mathbf{T} & \mathbf{K} \\ \mathbf{K} & \mathbf{T} \end{pmatrix} + \begin{pmatrix} V_1(R) - \frac{1}{4}\alpha_{11}(R)\epsilon^2(t) & -\frac{1}{2}\mu_{12}(R)\epsilon(t) \\ -\frac{1}{2}\mu_{12}(R)\epsilon(t) & V_2(R) - \hbar\omega(t) - \frac{1}{4}\alpha_{22}(R)\epsilon^2(t) \end{pmatrix} \quad (1)$$

where \mathbf{T} is the kinetic energy, \mathbf{K} takes into account non-adiabatic couplings and $V_j(R)$ are the electronic potential energy curves. The dynamical phases in the coupling (off-diagonal term in the Hamiltonian) are moved by a unitary transformation to the energies, showing photon-shifted potentials. In Eq.(1) we have assumed that the field may be resonant or quasi-resonant between the two electronic states, coupled via the dipole moment μ_{12} , and nonresonant with respect to the remaining states of the molecule. The effect of the remaining states on the two selected states is described in terms of the quasi-polarizabilities (α_{11} and α_{22}) up to the next leading order in the field, ϵ^2 . They account for the Stark shifts. In principle, two very different fields (with very different frequencies) could be responsible for the electronic coupling and the Stark-shifts. In more general scenarios, the quasi-resonant electronic transition could require multiphoton absorption instead of the single photon absorption used in Eq.(1).

We consider now two different regimes depending on whether the effect of the laser on the potentials renders a "soft" or "hard" shaping. The first one is characterized by the lack of a resonant or quasi-resonant excitation so that the off-diagonal terms are negligible. Then the initially populated LIP can be written as

$$V_1^a(R, \epsilon) \approx V_1(R) - \frac{1}{4}\alpha_{11}(R)\epsilon^2(t)$$

in which α is the dynamic polarizability, taking into account the effect of all the remaining states. In some cases the polarizability is dominated by a single electronic state, closer in energy to $V_1(R) + \hbar\omega$. In other cases, the frequency is much smaller (*e.g.* an infrared laser or an electric pulse) and the static polarizability can be used instead. Unless $\alpha_{11}(R)$ changes drastically around the equilibrium geometry of $V_1(R)$ (or the regions where the probability of finding the nuclear wave function are larger), the topological changes in $V_1(R)$ induced by the field will be small, hence the "soft" character of the shaping. The control is mainly exerted by $\epsilon(t)$, inducing energy variations (Stark shifts) of the potential. It is often the case that the ground LIP is very similar to the ground molecular potential. Most interesting effects occur in excited LIPs. One first needs to move the population to an excited potential such that the events happen in V_2^a .

On the other hand, when the interaction is quasi-resonant, as a first approximation one can typically neglect the polarizability and concentrate on the two crossing potentials. The LIPs are obtained by diagonalizing

the potential energy operator, including the field coupling. They are the instantaneous eigenstates of the electronic Hamiltonian. Applying the rotation matrix

$$\begin{pmatrix} \cos \theta(R; \epsilon) & \sin \theta(R; \epsilon) \\ -\sin \theta(R; \epsilon) & \cos \theta(R; \epsilon) \end{pmatrix}$$

where $\theta(R; \epsilon)$ is the rotation or mixing angle that diagonalizes the matrix, we obtain

$$\mathbf{H}^{\text{DS}} = \begin{pmatrix} \mathbf{T} & \mathbf{K}' \\ \mathbf{K}' & \mathbf{T} \end{pmatrix} + \begin{pmatrix} V_1^a(R; \epsilon) & i\dot{\theta} \cos 2\theta \\ -i\dot{\theta} \cos 2\theta & V_2^a(R; \epsilon) \end{pmatrix} \quad (2)$$

The off-diagonal terms in the kinetic operator, \mathbf{K}' are often referred to as *spatial* non-adiabatic terms, while those in the potential operator are *dynamical* non-adiabatic terms. They depend on the time-derivative in the mixing angle, $\dot{\theta}$, which reflects the time-variation of the field, $\dot{\epsilon}(t)$. When the pulses are strong enough and their time evolution is slow enough (in comparison with the motion of the nuclear wave functions) the off-diagonal terms can be neglected. Then, if at initial time (when $\epsilon(0) = 0$) the initial potential correlates with a single LIP, $V_1^a(R; \epsilon(0))$, all the dynamics will occur in this LIP and the final electronic state as well as all the properties of the system during all times, will solely depend on $V_1^a(R; \epsilon(t))$. In order to characterize the LIP we need to know the structure of the strongly coupled electronic potentials, V_1 and V_2 . It is most important to localize the LIAC, R_c , defined by the condition

$$\Delta(R_c, t) = V_2(R_c) - V_1(R_c) - \hbar\omega(t) = 0. \quad (3)$$

The populated LIP can be expressed as a function of the original molecular potentials, as

$$V_1^a(R, \epsilon) = \cos \theta(R, \epsilon) V_1(R) + \sin \theta(R, \epsilon) V_2(R) \quad (4)$$

where the mixing angle θ changes from 0 to $\pi/2$ at both sides of the avoided crossing, R_c . The first important effect that such an avoided crossing has in the LIPs is to completely deform the molecular potential energy curves and thus to change the structure of the molecule. For $V_1^a(R)$ the LIP looks like $V_1(R < R_c)$ before the crossing and like $V_2(R > R_c)$ after it. Through the LIAC, the nuclear wave packet can transfer part of the population. It operates in analogous way to a molecular (beyond Born-Oppenheimer-like) internal conversion, induced by \mathbf{K} . In the adiabatic limit, which requires a large energy gap between the LIPs in the LIAC and slow changes in the pulse envelope $\epsilon(t)$, the population in the initial electronic state

is given by $\cos^2 \theta(R, \epsilon)$, while the population in the other coupled electronic state is given by $\sin^2 \theta(R, \epsilon)$. Therefore, the motion of a nuclear wave packet across R_c in $V_1^a(R, \epsilon)$ represents full population transfer from V_1 to V_2 .

We will now briefly mention some features of population transfer analyzed from the perspective of LIPs. As noticed, one of the most important steps in the design of laser control schemes is to localize the LIAC of the LIP, as this topological point is an indication of possible population inversion. In order to fully transfer the population from V_1 to V_2 one needs to modulate θ via the control field $\epsilon(t)$. However, depending on the structure of the LIP and the initial kinetic energy, the nuclear wave function will be able or not to cross the region of the potential that correlates with V_2 . In the most simple cases, as *e.g.* in population transfer from a bound to a dissociating electronic state, a chirped pulse where the pulse frequency $\omega(t)$ sweeps through the Franck-Condon region is often enough to allow the mixing angle $\theta(R, \epsilon)$ to change from 0 to $\pi/2$ for all values of R where the wave packet is located. Therefore, most LAMB schemes use chirped pulses. In other cases, one needs to find a more difficult adiabatic path that connects V_1 to V_2 via the LIP, requiring a more elaborate trajectory of $\theta(R, \epsilon)$. Typically, when the equilibrium geometries of V_1 and V_2 are very separated and the energy gap between the LIPs at the LIAC is large, one needs to find additional electronic states that allow to modulate the LIP from V_1 to V_2 adiabatically. The APLIP scheme using time-delayed pulse sequences, or the CARP scheme, using chirped pulses, control the population inversion to a higher excited state by means of two-photon absorption. This requires the use of more than one control pulse, therefore adding challenges to the experimental implementation of the scheme.

If the population transfer is fully adiabatic, there is no internal barrier in the adiabatic pathway at the bottom of the LIP connecting the initial equilibrium geometry corresponding to V_1 and the final equilibrium geometry corresponding to V_2 . Under these circumstances the transfer preserves the form of the nuclear wave function. In particular, the dynamics conserves the vibrational quanta. In APLIP, this is possible by using two control pulses, one called the pump pulse $\epsilon_p(t)$, the second one called the Stokes pulse $\epsilon_S(t)$. For instance, consider that we want to invert the population in Na_2 from the ground $X^1\Sigma_g^+$ state (V_1) to a second excited $2^1\Pi_g$ state (V_2), using a resonant two-photon transition through the intermediate $A^1\Sigma_u^+$ state (V_b), whose equilibrium geometry lies in between that of the initial and the final state (although this is not an essential requirement for the intermediate state, it typically reduces the pulse intensities needed for the APLIP scheme). Garraway and Suominen[51] showed that a counter-intuitive pulse sequence with $\epsilon_S(t)$ preceding $\epsilon_p(t)$ could lead to full population inversion without populating the intermediate state at all. This is possi-

ble because such pulse sequence prepares a LIP called V_d^a , $V_d^a = \cos \theta V_1 - \sin \theta V_2$, that never correlates with the intermediate potential V_b . Also interestingly, in this LIP the Stark effects induced by both control pulses are minimal regardless of the pulse strength. With different properties, other APLIP pulse sequences allow full adiabatic passage[54, 55].

In the following subsections we will analyze several examples of theoretically proposed schemes of control exerted via Stark effect (that is, when the coupling is far off-resonant and at least as a first approximation one can use the polarization), and control exerted by LIP shaping (when the coupling is resonant or quasi-resonant and one has to take into consideration substantial population transfer). In the latter, the geometrical factors are obvious, as the population transfer is typically encoded in the reshaping of the LIP, but the dynamics play also a very important role on the creation, passage or destruction of the LIPs.

CONTROL OF MOLECULAR GEOMETRY BY SHAPING BOUND WITH DISSOCIATIVE POTENTIALS

In this section we will review several schemes based on LIPs that were designed to control the bond length of diatomic molecules. In general, a molecule has different equilibrium geometries in each electronic state. Typically, the bonds are more relaxed in the excited states. Therefore, by electronic absorption with strong ultra-short pulses, it is possible to transfer all the initial wave function to the excited state, creating a wave packet of vibrational eigenstates after the pulse is switched off. This vibrational wave packet oscillates around the excited-state equilibrium geometry of V_2 for a few periods so that the bond length of the molecule will be well defined until dispersion occurs. As the dynamics is driven by the molecular potential, there is little control over the period or amplitude of the motion.

Alternatively, the electronic absorption may proceed adiabatically, as in APLIP. Then the nuclear wave function will be slowly transferred to the equilibrium geometry of the second excited electronic state. During this process, at every intermediate time the bond length is well defined, as the wave function sits in the bottom of a single LIP. The idea behind the LAMB scheme is precisely to stop or freeze the transport process at the desired intermediate bond length. As long as the pulses remain constant, so will the bond length. However, the potential range for the control is much larger when the final electronic state is dissociative, since then its equilibrium geometry is at $R \rightarrow \infty$. Hence, in principle, one can prepare the molecule at any bond length larger than the initial one. However, the adiabaticity of the process deteriorates for very large bond distances, and the disso-

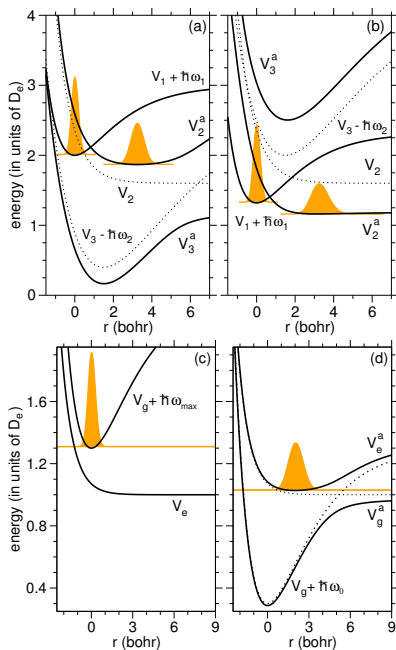


FIG. 1: Different scenarios of the LAMB scheme using one and two pulses. Dotted lines are the molecular potentials and solid lines are the potentials in the presence of the field (the LIPs plus the uncoupled V_1 potential). In (a) and (b) we show LAMB schemes using a chirped and a transform-limited pulse, blue-shifted or red-shifted with respect to the $V_2 \rightarrow V_3$ transition, respectively. In (c) and (d) the mechanism of LAMB with a single chirped pulse is represented. At initial times the pulse frequency must be blue-shifted from the photodissociation band, while at later times, the red shifted frequency, after sweeping all the photodissociation band, sets the new "equilibrium" bond distance. (From J. Chem. Phys. 134, 144303, fig.1)

ciation probability becomes non-negligible.

The first proposed implementation of LAMB assumed that the initial potential V_1 and the intermediate potential V_3 , where both bound potentials, coupled via a pump pulse $\epsilon_1(t)$, while the target electronic state V_2 was dissociative, coupled to the intermediate one via $\epsilon_2(t)$. Following one possible APLIP sequence but shaping $\epsilon_2(t)$ such that instead of switching it off, the pulse remains at a plateau amplitude ϵ_0 for a certain time, it was possible to elongate the bond[83].

More natural LAMB implementations are possible when V_2 is coupled directly to the initial state V_1 [84, 85]. Fig.1 outlines both two-pulse as well as one-pulse scenarios. In the first case the LAMB process implies the following mechanism: Initially $\epsilon_2(t)$ is switched on, with an off-resonant frequency that prepares the LIP V_2^a with a LIAC between V_3 and V_2 at the desired bond length. Then, while $\epsilon_2(t) = \epsilon_0$ remains constant, another pulse, $\epsilon_1(t)$, moves all the population from V_1 to V_2 , which in the presence of ϵ_0 is V_2^a . This electronic absorption can pro-

ceed rapidly, using an ultrashort transform-limited pulse that generates a nuclear wave packet moving in the LIP. In this case we talk of a vertical wave function transfer (VWT). Or it can be quasi-static, using a chirped pulse, in which we talk of an adiabatic transfer. In both cases full population inversion requires pulse bandwidths $\Delta\omega_1$, at least as large as the absorption band, $\Delta\omega_{FC}$. In fact, in the quasi-static case, the chirp typically needs to span an even larger bandwidth. Fig.1 (a) and (b) show how the shape of V_2^a is influenced by the choice of ω_2 , blue-shifted or red-shifted with respect to the $V_2 \rightarrow V_3$ transition. In the first case there is properly a LIAC and the bond length in V_2^a is better defined. In the second case there is no proper LIAC and the control is mostly done by Stark effect. Then the LIP is much flatter and it is more difficult to achieve adiabatic population transfer.

On the other hand, it is possible to use a single chirped pulse, $\epsilon(t)$, responsible for both roles: the adiabatic transfer and the formation of the LIP. The basic mechanism is explained in Fig.1 (c) and (d). At initial times $\omega(0)$ must be blue-shifted from the absorption spectrum to the dissociative state V_e . Slowly sweeping through the photodissociation band the population is transferred in a quasi-static way, with the wave packet always located at the bottom of the LIP. Then the chirp must sweep through all the emission spectra. The final value of the frequency, ω_0 , defines the LIAC and the bond length[87]. If ω_0 is not small enough, $V_e(R_c) - V_g(R_c) - \hbar\omega_0$ will sit at short R_c . On the other hand, when $\hbar\omega_0 \sim D_e$ (where D_e is the bond energy in V_g), the LIAC is at infinite distance. One can therefore measure the required bandwidth scaled with respect to D_e . Using a single pulse, $\Delta\omega$ must be of the order of D_e .

In comparison with a VWT process a typical LAMB process requires 10 to 100 more energy (integrated pulse amplitude or peak amplitude times duration) from the pulses. The extra energy is mainly used to deform the potential. This pays off in the fact that the molecular properties associated to the wave packet dynamics, is entirely governed by the field parameters. In particular, any *trajectory* in the "chirp function" $\omega(t)$ entails different excursions of the average internuclear distance, or bond length. For instance, any time-symmetric function $\omega(t)$ leads to fully reversible bond elongations that mimic a single period of a classical molecular vibration, with both the amplitude and frequency of the vibration being externally controlled[89]. If $\omega(t)$ is periodic, the inverse of its period will be the "frequency" of this LIP-supported vibration[88].

In Fig.2 we show a numerical example of the reversible control of the bond elongation. It can be observed that the nuclear wave function is always in the ground state of the LIP. The exchange of kinetic energy into zero energy of the LIP needs time to allow the nuclear wave function to adjust its width to the width of the potential. Hence, only "slow" vibrations can be adiabatically con-

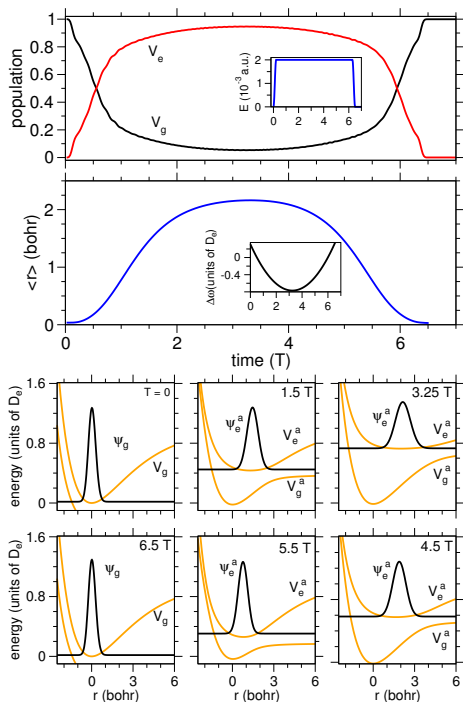


FIG. 2: Dynamics of the system under a parabolic chirped pulse in adiabatic conditions. Time units are scaled with respect to the fundamental vibrational period in the ground potential, T , whereas the pulse duration is $\tau = 6.5T$. (top) The dynamics of electronic populations and bond length. Insets show the pulse shape (upper inset) and the laser detuning (lower inset). (bottom) Snapshots of the adiabatic wave function, remaining in the bottom of the LIP at all times. By chirped induced population inversion, V_e^a correlates at initial and late times with the initial potential, V_g . (From Phys. Rev. A 82, 063414, Fig.2.)

trolled, where the period of the vibration is much larger (typically 5 or more times larger) than the characteristic vibrational period of the ground state, T . For a Morse oscillator $V = D_0(1 - e^{-\beta(R-R_0)})^2$ of reduced mass m , $T = \sqrt{2m\pi^2/D_0\beta^2}$. If $\omega(t)$ changes faster than this characteristic period of time the process is not fully adiabatic. As Fig.3 shows, the breakdown of adiabaticity implies that the nuclear wave function receives some kinetic energy, such that the motion of the bond length depends partially on the LIP equilibrium geometry determined by $\omega(t)$, and partially on the vibrational motion of the nuclear energy on this LIP[90]. When the chirp is reverted one prepares a highly excited vibrational wave packet in the ground potential. However, if $\omega(t)$ varies too fast, the wave packet has little time to move from its initial position and the gained vibrational energy is small.

The simplest procedure to prepare large amplitude vibrations (albeit with uncontrollable periods) is to use a two-pulse LAMB scheme. While the control pulse prepares the LIAC and determines the equilibrium bond dis-

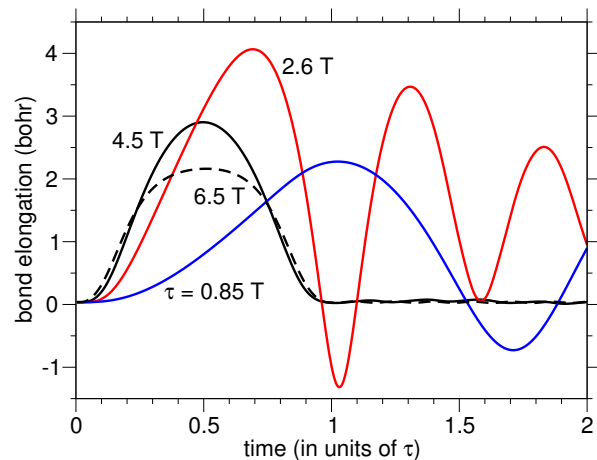


FIG. 3: Bond dynamics as a function of time scaled with the pulse duration τ . In the strong adiabatic regime ($\tau \geq 6T$), the time-scaled bond dynamics are similar and follow the same curve. Before fully adiabatic conditions ($\tau = 4.5T$), the dynamics is still time-symmetrical but the bond stretches more at half the pulse duration. For shorter pulses the bond dynamics is anharmonic. The wave packet gains momentum, and it is no longer attached to the bottom of the LIP. The bond can be further stretched, and as the chirp is reversed ($t/\tau > 0.5$), the wave function returns to the initial potential as a vibrationally excited wave packet. If the pulse is too short, however, the wave packet has not time to reach the classical turning point before the chirp reverses and the LIP converges to the initial potential. (From J. Phys. Chem. A 116, 2691, Fig. 3.)

tance, one can rely on VWT processes to excite the wave function from V_1 to the LIP. Some control on the amplitude of the vibration can be achieved by selecting the timing and frequency of the ultrashort transform-limited pulse[86], as shown in the next section.

THE ROLE OF THE ELECTRONIC CHARGE

While the nuclear wave function encodes the molecular structure, given by the shape or the geometry, the electronic distribution is responsible for the chemical properties. In particular, the dipole moment typically provides simplified information regarding the distribution of charges. Based on the Born-Oppenheimer approximation, in the previous section we have focused on the control of the nuclear wave function by means of LIPs. Here, we analyze the role of the electronic wave function and of electron-nuclear dynamics[97, 99, 100].

In a LAMB process, the total wave function of the system is a coherent superposition of both nuclear and electronic wave functions[87],

$$\Psi(R, q, t) = \phi_g(R, t)\Xi_g(q; R) + \phi_e(R, t)\Xi_e(q; R) \quad (5)$$

However, in a fully adiabatic evolution, the nuclear wave

packet in V_g and V_e have the same shape, $\phi_g(R, t) \propto \phi_e(R, t) \propto \phi^a(R, t)$, so that we can write

$$\begin{aligned}\Psi(R, q, t) &= \phi^a(R, t) [a_g(t)\Xi_g(q; R) + a_e(t)\Xi_e(q; R)] \\ &= \phi^a \Xi^a(q, t; R)\end{aligned}\quad (6)$$

where $\Xi^a(q, t; R)$ is the dressed electronic wave function that gives the LIP force field. The total wave function is thus separable and not an entangled state of nuclear and electronic states. Since the total wave function in the LIP is a single Born-Oppenheimer product, there is perfect correlation between the electronic and nuclear motion. Notice that the changes of the electronic wave function are externally controlled: they do not rely on dynamical phases as in superpositions of different elec-

tronic states. Adiabaticity is required for the single product wave function to faithfully represent the dynamics. Hence the changes in the LIP must be slower than the typical time-scale of the nuclear dynamics. The perfect correlation of electronic and nuclear motion in the LIP is only possible because the electron dynamics occurs in the time-scale of the nuclear dynamics.

In order to analyze the type of electron changes conveyed by the transformation of the LIP and the possible effects of electron-nuclear motion, one needs to use a model that allows integrating the full time-dependent Schrödinger equation beyond the Born-Oppenheimer approximation. In the following, we use a well-known 1+1D Hamiltonian often employed to characterize the dynamics of the molecular Hydrogen cation under strong fields[97–100],

$$H = -\frac{\hbar^2}{2\mu_e} \frac{\partial^2}{\partial z^2} - \frac{\hbar^2}{M} \frac{\partial^2}{\partial R^2} - \frac{1}{\sqrt{(z - \frac{R}{2})^2 + 1}} - \frac{1}{\sqrt{(z + \frac{R}{2})^2 + 1}} + \frac{1}{R} + q_e z \epsilon(t) \quad (7)$$

where z is the electron coordinate, R is the internuclear distance, M is the mass of the proton, $\mu_e = 2m_e M / (2M + m_e)$ is the reduced mass of the electron, which is approximately the electron mass m_e , and $q_e = (2M + 2m_e) / (2M + m_e) \approx 1$. It should be noted that this Hamiltonian includes all non-adiabatic couplings (i.e., the Born-Oppenheimer approximation is not used) although the electron is forced to move along a line defined by the bond axis through the approximated soft-core Coulomb potential[112–114]. More elaborate Hamiltonians and calculations exist[115, 116].

In Fig.4 we show results of the actual dynamics obtained by solving Eq.(7) under a strong constant field ϵ_0 . As the initial state, $\Psi(z, R, 0) = \varphi(R, 0)\psi_1^{BO}(z; R)$, we consider a nuclear wave function with the same probability density as the ground state of H_2 in the ground electronic state of the ion H_2^+ , essentially assuming an instantaneous ionization process[97]. Since the bond length in H_2 is shorter than in H_2^+ , the ground state of the former is a nuclear wave packet moving in the ground electronic state of the cation, $1\sigma_g$. An ultrashort pump pulse of $\tau = 1$ fs duration and carrier frequency $\omega_p = 5.4$ eV, with peak amplitude $\epsilon_p = 0.05$ a.u. at $t_0 = 6$ fs is then switched on. The duration, frequency, and intensity are chosen to maximize population transfer from $1\sigma_g$ to the first excited electronic state $1\sigma_u$ (henceforth in the section, V_1 and V_2). The envelope of the pulse is chosen as a cosine square pulse, $\epsilon_p(t) = \epsilon_p \cos^2(\pi(t - t_0)/\tau)$ for $-\tau/2 \leq t - t_0 \leq \tau/2$.

As in a typical two-pulse LAMB scenario, during all

times the control field is present. In this calculation we use a *DC* electric field $\epsilon_0 = 0.015$ a.u. Then the dynamics proceeds in the so-called field-induced potentials (FIPs) U_1 and U_2 , which are analogous to the LIPs but using constant fields. U_1 shows bond softening. For large fields ($\epsilon_0 \geq 0.03$ a.u.) the wave packet kinetic energy can be above the ground state bond energy. On the other hand U_2 shows bond hardening. Indeed, in the presence of an external field, H_2^+ (or any other symmetrical molecular cation) has charge resonance states[117, 118]. The transient dipole increases with distance and it is possible to stabilize the molecule at very large bond lengths. For the chosen parameters, the population in V_2 is ~ 0.7 after the pump pulse, while the ionization and dissociation probabilities are both below 10%. Using more intense DC fields ($\epsilon_0 > 0.04$ a.u.), the ionization and dissociation probabilities increase.

Fig.4 shows how the motion of the electron and protons is clearly correlated, with the electron departing from between the two protons, to the right proton (the one at positive z) as the protons move apart. The period of both motions is practically the same. The mechanism under this correlation is shown in Fig.5, where we show different snapshots of the soft-core Coulomb potential sliced at the internuclear distance where the probability of finding the nuclear wave function is larger. Also shown is the electronic wave function. As the bond enlarges the electron follows the right nuclei. With the chosen field parameters, the average internuclear distance reaches 14 a.u. [Fig.4(b)] while the electron average distance and hence

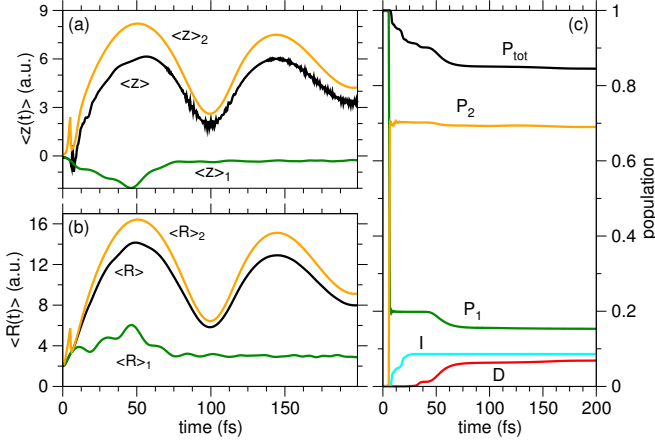


FIG. 4: (a) Average electron position and (b) average internuclear distance as functions of time. (c) Probability as a function of time for dissociation (D), ionization (I) and the population remaining in the U_1 and U_2 FIPs, P_1 and P_2 , respectively. (J. Chem. Phys. 139, 084306, Fig.2.)

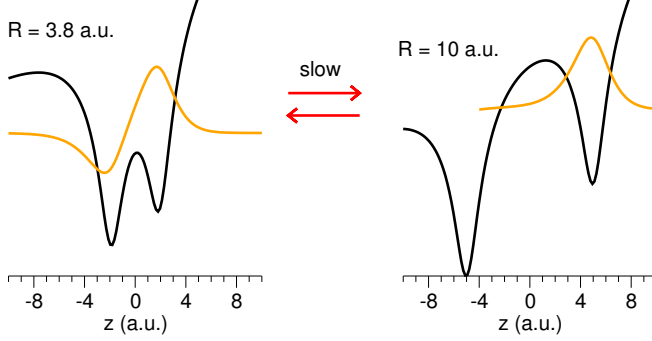


FIG. 5: Sketch of the success of the mechanism for the creation of the dipole starting from the excited FIP. We show slices of the wave function and the soft-core Coulomb potential coupled with the field for two different internuclear distances which correspond to the initial state and at maximum bond stretch. Initially the electron is mainly localized on the right atomic well. As the protons separate, as long as the energy of the wave function is below the ionization barrier, the electron remains with the right proton and moves in the time scale of the vibrational motion. (From J. Phys. B 48, 043001, Fig.7.)

the electric dipole reaches 6 a.u. [Fig.4(a)]. In fact, the wave packet reaches quite longer distances in z and R than those indicated by the average. Since the FIP is very anharmonic the dephasing makes the wave packet spread quickly. The maxima and minima of $\langle R(t) \rangle$ and $\langle z(t) \rangle$ become less pronounced after a few periods, until the wave packet fully disperses and the average internuclear distance remains constant. This is the so-called collapsed state. For weak DC fields (and weaker bonds), there can be as few as 2 periods before the system reaches the collapsed state, whereas for stronger fields one can easily observe 10 periods of motion. In principle, at larger times

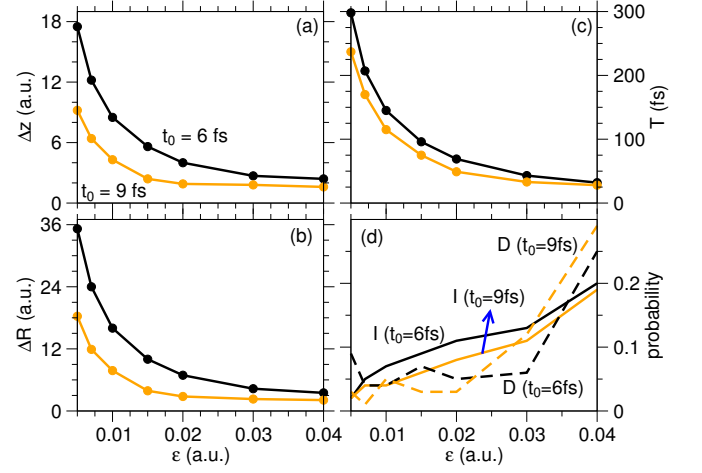


FIG. 6: (a) Amplitude of the dipole, (b) bond elongation, (c) dipole period, and (d) probabilities of dissociation and ionization as functions of the amplitude of the field ϵ_0 for different time-delays of the pump pulse t_0 . (From J. Chem. Phys. 139, 084306, Fig.3.)

one could expect the revival of the periodic motion[99]. The maximum dipole that can be achieved is also limited by imperfections in the population transfer between the FIPs, since the electron remaining in U_1 moves in the opposite direction (with the left proton) making the averages calculated on each FIP, $\langle z \rangle_j$ and $\langle R \rangle_j$ ($j = 1, 2$) shown in Fig.4.

Still, extremely large electronic dipoles and bond elongations can be achieved. Defining Δz as the range of the dipole motion, $\Delta z \equiv \langle z(t_{max}) \rangle - \langle z(t_{min}) \rangle$, where t_{max} is the time at which $\langle z \rangle$ reaches its first maximum and t_{min} is the time at which $\langle z \rangle$ is at a minimum during the first period, and similarly for the bond elongation ΔR , in Fig.6 we show how Δz , ΔR , and the period of the dipole T change as functions of ϵ_0 and t_0 , together with the probabilities of dissociation and ionization. For the range of parameters where the ionization and dissociation probabilities are small, one can generate dipoles that reach as large as 40 Debye, oscillating at slow vibrational motion. The period of these dipoles varies from ~ 300 fs down to 25 fs, i.e., over an order of magnitude. These correspond to frequencies in the far infrared, from 3 to 40 THz approximately.

It is possible to use a low frequency laser pulse instead of a constant field, but then the pulse must meet very specific conditions[100]. In particular, its frequency must be approximately equal to the frequency of the vibrational motion in the LIP. Otherwise, the correlation between the motion of the electron driven by the field, and that of the protons, oscillating in the potential, is not perfect. In this scenario, the LAMB dynamics is that of an electron moving along with one proton as the bond stretches, and hopping to the other proton as the bond

compresses. Basically, we have a proton loosely attached to an Hydrogen. Depending on the phase of the electric field, the Hydrogen and proton exchange their role. It is crucial that the bond is maximally compressed when the amplitude of the oscillating electric field is zero as otherwise the electron cannot hop from one proton to the other, leading to dissociation.

We have shown that the electron-nuclear correlation is an essential condition to create large-amplitude oscillating dipoles. Although in principle any superposition of electronic states of different parity, such as $\Psi(z, R, 0) = \varphi(R, 0) (\psi_1^{BO}(z; R) + \psi_2^{BO}(z; R)) / \sqrt{2}$, induces an oscillating dipole, the dipole in this case quickly decays due to the dephasing of the nuclear and electron motion[99]. Alternatively, a high frequency laser pulse can be used to drive the electron in the ground state creating a fast oscillating dipole, but this dipole can only be small as the excursion length of the electron in the field (the displacement that the electron can reach before the electric field changes its sign) is necessary small in the ground potential under optical driving frequencies. For lower frequencies the excursion length and the induced dipole could be larger, but tunneling ionization dominates[100].

In summary, we have shown that in order to create an oscillating electric dipole in a homonuclear diatomic cation without an oscillating driver one needs (i) to break the symmetry of the system and (ii) to sustain highly correlated electronic and nuclear motion, which are guaranteed by the LAMB dynamics.

CONTROL OF PHOTODISSOCIATION BY SHAPING TWO DISSOCIATIVE POTENTIALS

Strong fields can also be used to control photodissociation reactions in the adiabatic regime. The first obvious effect is the Stark shift of the photodissociation bands, thus changing the spectrum[119]. If several dissociation channels are present, one can use a pump pulse in combination with a strong nonresonant pulse to separate the different channels[110]. However, the field also couples the different excited states so that the dissociation occurs on a "mixed" channel, that is, on a superposition of excited electronic states correlating to different channels[110, 111]. In this section we review some proposals that we have presented to achieve control over different reaction observables, such as the yield and the kinetic energy distribution of the fragments[111], by using strong nonresonant pulses. In the chosen examples the LIPs are formed between two dissociative potentials that never cross. Since there are no LIACs and no population inversion, the LIPs only show "soft" shaping.

Control of photodissociation spectra

Using an ultrashort pump pulse with carrier frequency ω_p , the absorption probability in a photodissociation band quickly decays when the absorption is nonresonant. Taking into account the pulse bandwidth $\Delta\omega_p$, in the absence of competing dissociating channels, the photodissociation probability is roughly given by [120]

$$P_j(\omega_p) \sim \exp \left[- \left(\frac{D_{j0} - \hbar\omega_p}{\hbar\Delta\omega_p} \right)^2 \right] \quad (8)$$

where $D_{j0} = V_j(R) - V_0(R)$ is the energy gap at the Franck-Condon (FC) region. However, using a strong non-resonant field ϵ_S in addition to the pump pulse, the electronic states are Stark-shifted. Under the same approximations we obtain a similar expression where instead of D_{j0} one needs to use the Stark-shifted energy gap

$$D_{j0}^p(\epsilon_S) = V_j^a(R) - V_0^a(R) \approx D_{j0} - \frac{1}{4} (\alpha_{jj} - \alpha_{00}) \epsilon_S^2 \quad (9)$$

The position of the photodissociation bands corresponding to different electronic channels can therefore be controlled. The control can be more effective when the polarizabilities α_{jj} have different signs for different electronic states, such that ϵ_S can both blue-shift and red-shift the different bands of the spectra.

As a numerical example we consider control on the photodissociation of the molecular ion ICl^- [121] shown in Fig.7. Assuming the molecule is aligned with ϵ_S (thus the symmetry rules associated to parity can be violated), the first two excited states, $^2\Pi_{1/2}$ (henceforth V_1) and $2^2\Pi_{1/2}$ (henceforth V_2), are dipole allowed from the ground state $^2\Sigma_{1/2}$ (V_0) and are the only accessible states below 3eV or 400nm. The two excited states, on the other hand, are too far apart to be reached by a single pulse (unless it is an attosecond pulse) and do not cross at different internuclear distances, so that internal conversion is negligible.

In Fig.8 we show the photodissociation spectra when the pump pulse is a 400 fs pulse of a TW/cm^2 in the range where the two bands are observed. The spectra barely depends on the parameters of the pump pulse. However, it changes considerably when a very strong nonresonant ϵ_S pulse is included. For the results of Fig.8 we have assumed that its frequency is negligible, that is, we have employed half-cycle pulses. The full width at half maximum (FWHM) of ϵ_S was chosen as 400 fs, which implies that the control pulse lasts about twice the duration of the pump pulse.

Interestingly, although for the chosen parameters α_{22} and α_{33} are both positive and of similar value, the spectral bands after ϵ_S are not only blue shifted. Indeed the high frequency edge of the band is blue shifted so that, for instance, with $\epsilon_S = 0.03$ a.u. the band for V_1 overlaps

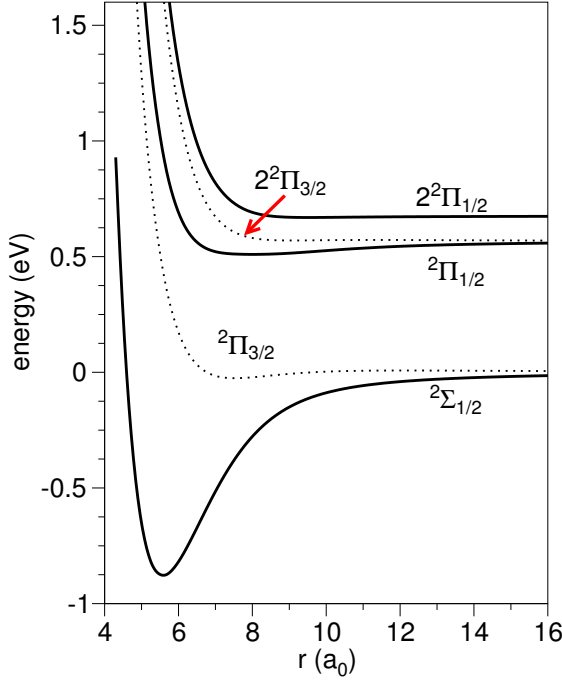


FIG. 7: Potential energy curves for ICl^- . The ground state is $^2\Sigma_{1/2}$. Up to 3.0 eV, the only two excited states that are coupled to the ground state by transition dipole moment are $^2\Pi_{1/2}$ and $^2\Pi_{3/2}$. (Adapted from J. Chem. Phys. 130, 124320, Fig.1.)

the spectral window of the band for V_2 in the absence of the pulse. However, the low-frequency edge of the bands remain practically the same as without the Stark-shift. This is because the pump pulse is also acting when ϵ_S is small (either at the head or trail of the pulse, depending on the time delay between the pulses), so that in the spectra one essentially records the yield of photodissociation for all possible Stark-shifts, obtained with $\epsilon_S(t)$ ranging from zero to its peak amplitude. A simple Stark-shift of the whole band would be observed for much larger control pulses when $\epsilon_S(t)$ straddles $\epsilon_p(t)$, such that $\epsilon_p(t)$ is switched on after and switched off before the control pulse.

Control of photodissociation yields.

In Fig.8 we showed the photodissociation spectra, with the expected band shifts. However, as indicated in Sec.2, when a strong pulse couples two states, the nature of the states change by virtue of the polarizability. In particular, there will be some probability that a nuclear wave packet dissociating at the band corresponding to V_1 will actually be in the excited V_2 state and viceverse. For an approximately constant $\Omega_S = \mu_{12}(R)\epsilon_S(t)$ the probabili-

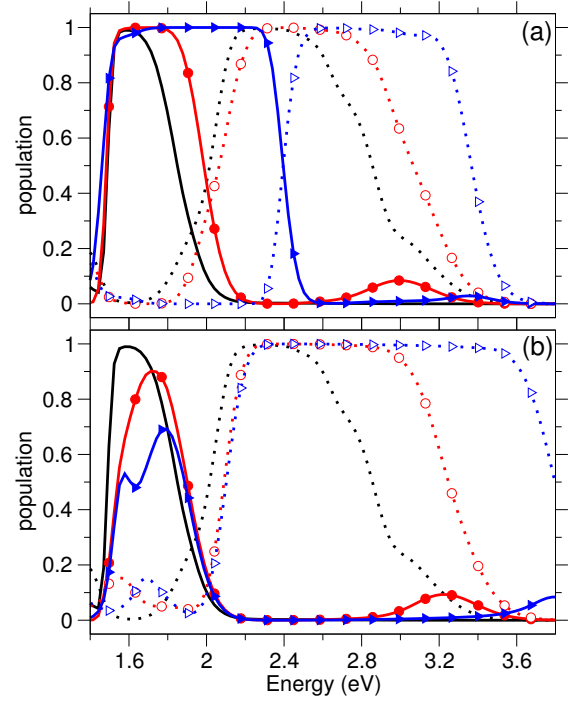


FIG. 8: Photodissociation spectra in the presence of the control pulse using the counterintuitive sequence with (a) $\epsilon_S(t) > 0$ and (b) $\epsilon_S(t) < 0$. The keys of the symbols are the following: Circles are results with peak amplitudes $\epsilon_S = \pm 0.02e/a_0^2$, triangles are results with Fig $\epsilon_S = \pm 0.03e/a_0^2$, and lines with no symbols are results with $\epsilon_S = 0$. The solid line gives dissociation in V_1 and the dotted lines dissociation in V_2 . The pulse parameters are given in the text. (Adapted from J. Chem. Phys. 130, 124320, Fig.6.)

ties are roughly given by

$$\chi = \frac{P_2}{P_1} \sim \left(\frac{\Omega}{2\Delta} \right)^2. \quad (10)$$

where Δ is the energy gap between the electronic states. The first question, then, is why in Fig.8 we observe only one product, the electronic channel corresponding first to V_1 and then to V_2 , at the two photodissociation bands. The reason is because we used a constant $\mu_{23}(R)$ and the control pulse was switched off slowly. Then the effect of the polarizability that occurred as $\epsilon_S(t)$ raised was reverted when the pulse decayed. Eq.(10) was only operative when the control pulse was switched on leading to transient effects, but it does not affect the asymptotic results.

However, when either $\mu_{12}(R)$ or $\epsilon_S(t)$ decay abruptly (such that $\Omega_S(t)$ decays abruptly) then the effect of the polarizability is no longer time-symmetrical and there are interesting effects that depend on the dynamics, that is, on the choice of the pulse sequence. We considered two cases: the PS sequence where $\epsilon_p(t)$ overlaps the head of $\epsilon_S(t)$ and the SP sequence, where $\epsilon_p(t)$ overlaps the trail of $\epsilon_S(t)$. In the results shown in Fig.9 we assumed

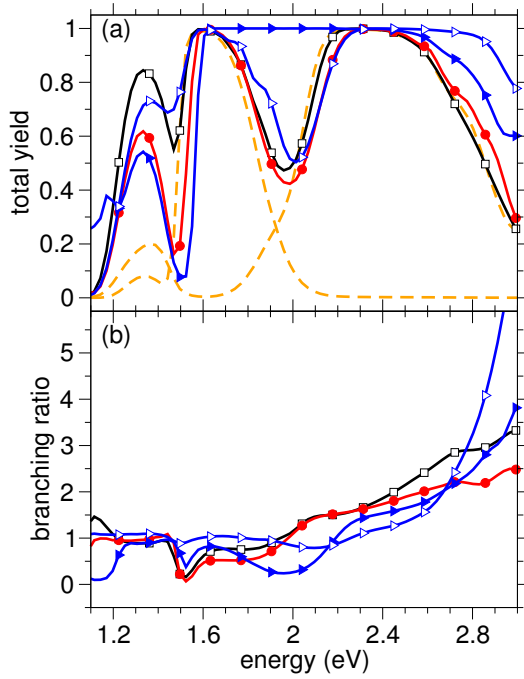


FIG. 9: (a) Photodissociation spectra in the presence of the control pulse using the intuitive sequence for different control peak amplitudes and (b) the resulting branching ratio $\chi = P_2/P_1$. In (a) we give the total yield of dissociation ($P_1 + P_2$). The peak amplitude of the control field for the different results is the following: In dashed line $\epsilon_S = 0$; in black line with squares $\epsilon_S = 0.01$; in red line with circles $\epsilon_S = 0.02$; in blue line with solid triangles $\epsilon_S = 0.03$ and in blue line with empty triangles $\epsilon_S = 0.03e/a_0^2$. All other parameters in the simulations are given in the text. (Adapted from J. Chem. Phys. 130, 124320, Fig.7.)

that $\mu_{12}(R)$ decayed abruptly. Similar results would be obtained using $\epsilon_S(t)$ with fast decay.

In the SP sequence the Franck-Condon excitation proceeds between V_0 and the spectrally chosen (by ω_p) excited molecular state V_e ($e = 1, 2$) but the dissociation occurs in the asymptotic region of the molecular potential, leading to selective dissociation. If the chosen potential V_e^a is *e.g.* V_2^a , then one collects all the fragments in the molecular state that correlates with that potential, that is, V_2 ,

$$\psi_0(R, t) \xrightarrow{S} \psi_2^a(R, t) \xrightarrow{P} \psi_2(R, t) \quad (11)$$

where ψ_j^a is the wave function initially in state j but of mixed electronic character by virtue of the Stark pulse. The SP sequence leads to the results shown in Fig.8. Conversely, in the PS sequence the Franck-Condon excitation occurs mainly in the excited molecular state e , selected by ω_p , but the dissociation occurs in the asymptotic region of V_j^a , leading to mixed dissociation. For

instance, if we initially excite V_1 ,

$$\psi_0(R, t) \xrightarrow{P} \psi_1(R, t) \xrightarrow{S} \psi_1^a(R, t) \propto \sqrt{\chi(\epsilon_S)} \psi_1(R, t) + \psi_2(R, t) \quad (12)$$

where χ is roughly given by Eq.(10). The labels 2 and 1 should be exchanged if we initially excite the system in the second photodissociation band, V_2 . In Fig.9 we show results of the photodissociation spectra using this sequence. In this case, the dynamics in the LIP mixes both dissociation channels. Fig.9(a) shows the overall yield of dissociation while Fig.9(b) shows the branching ratio. Quite naturally, the band at lower frequency corresponds to excitation in the V_1^a and leads to maximal dissociation in V_1 , while the band at higher frequency corresponds to excitation in V_2^a and leads to maximal dissociation in V_2 .

Clearly, regardless of the pump pulse, the timing of the control pulse with respect to the pump pulse affects the yield of the photodissociation reaction. However, one needs to work on resonance to create LIACs and fully invert the electronic populations to have more ample control over the branching ratios.

Control of the kinetic energy distribution.

The use of a strong nonresonant control field can lead to an important shift of the kinetic energy distribution (KED) of the fragments. At final time the wave packets move in either V_1 or V_2 and the maximum relative speed will be given by the energy difference between the FC window of the chosen excited LIP, $V_e^a(R)$, and the asymptotic value of the molecular potential to which it correlates, $V_e(\infty)$. If ϵ_S is large, then V_e^a is largely blue shifted. As the carrier frequency of the pump ω_p , is constant, the energy difference between the Franck-Condon region and the asymptotic threshold, which is fixed as $V_e(\infty)$, is smaller. Therefore, for constant ϵ_S one can achieve red-shifting of the KED.

In addition, using control pulses $\epsilon_S(t)$, the Stark-shifted KED will be very broad, like the photodissociation bands shown in Fig.10. Since during the absorption $\epsilon_S(t)$ is varying with time, the KED comprises energies available when $\epsilon_S(t) = 0$ (that is, in the absence of control pulse) to energies available when $\epsilon_S(t)$ is at its peak value, which are greatly red shifted.

A most interesting effect is the ability to detect a similar KED in both excited electronic states in the same experiment. The previous protocol of a PS sequence that allows to control the yield of the direct photochemical reaction enables this possibility. In the results shown in this section we will use half cycle control pulses $\epsilon_S(t)$ ($\omega_S = 0$) with very fast (~ 5 fs) switch off times, implying the sudden change of the wave packet from $\psi_e^a(t)$ to $\psi_1(t)$ and $\psi_2(t)$, both initially opened, and the initially closed electronic channels. Instead of changing the peak

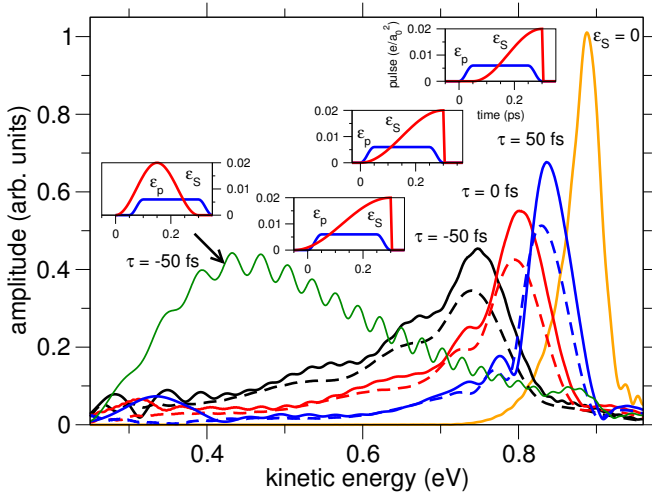


FIG. 10: Kinetic energy distributions of the relative motion of the fragments as a function of the time-delay between the pump and control pulses. The pulse sequences are shown in insets. The control pulse provokes broadening in the KED with different asymmetries for the PS and the SP sequences. In the PS sequence the solid-line curve shows the KED in the electronic state V_2 , and a dashed-line curve shows the KED in the electronic state V_1 . The distributions for the different electronic channels almost overlap owing to the dynamics in the same Stark-shifted potential. Because the control pulse is very intense the probabilities on both channels are not very different. The peaks of the distributions are always red-shifted with respect to the control free case, owing to the blue-Stark shift of the V_2 excited potential. (From J. Chem. Phys. 131, 204314, Fig.4.)

amplitude of ϵ_S , the control will be exerted by changing the time-delay between the pulses. Using the same ICI⁻ model introduced before, in Fig.10 we show the control exerted on both KEDs, which are practically identical for both products.

All the KEDs using the PS sequence exhibit a kind of asymmetry to the red, with the low-energy tail much larger than the high-energy tail. This is because in the PS sequence the absorption induced by $\epsilon_p(t)$ occurs mainly when $\epsilon_S(t)$ is small, and thus the potentials are only slightly blue-shifted. Blue-shifted asymmetries occur using the SP sequence. Then the bulk of the wave packet is excited when $\epsilon_S(t)$ is large, so that the peak of the KED is now much more red shifted. As explained in the previous section, in this case the photodissociation is selective and only one final state is observed. In the example shown in Fig.10 the peak of the KED is now close to 0.4 eV implying a larger deviation ($> 30\%$) of the relative speed of the fragments. We observe additional features, like the characteristic structure of interference due to excitation of the wave packet to the dissociative potential at different times [122].

In very nonresonant conditions, the manipulation of the KED relies solely on the ability to Stark-shift the

potential at the Franck-Condon region. In most cases, under reasonable pulse intensities, the expected effect will be small, as the Franck-Condon window typically lies in the fast-exponential repulsive wall of the potential and cannot be largely shifted in the same way that the absorption spectra cannot be greatly altered. However, using resonant control pulses between V_1 and V_2 leads to a full reshaping of the LIP. The key then for being able to change the asymptotic KEDs relies on non-adiabatically disrupting $\Omega_S(t)$ during the wave packet evolution through the reaction coordinate. Then the energy differences between $V_e^a(R)$ and the molecular potentials $V_1(R)$ and $V_2(R)$ at the time of the sudden switch off of $\epsilon_S(t)$ will be imprinted in the final KEDs [10].

CONCLUSIONS

In this review we have provided an overview of the theoretical framework that allows to describe and interpret many dynamical processes of diatomic molecules under the influence of strong laser fields, acting below the threshold of ionization. We have analyzed several theoretical proposals using laser schemes that allow to enlarge the bond length of molecules, to fabricate slow coherent vibrations, to generate huge transient dipole moments and to control the yield, branching ratio and kinetic energy distribution of the fragments after a direct photodissociation reaction. We have illustrated these proposals with results taken from some of our contributions in the field.

The experimental realization of some of these proposals is still lacking. It is typically difficult to find systems where the effect of the field is strong enough to deform the molecular potentials, yet not as strong as to completely ionize the molecule. Some of the proposed schemes also rely on frequency modulation over a bandwidth larger than what is possible with currently technology. More tests are needed, particularly in polyatomic molecules, to assess the validity of the approximations involved and to discover new ways to minimize the impact of ionization. However, recent experiments have shown that it is possible to achieve unprecedented control over photodissociation reactions[8–10]. The LIPs provide a new playground where essentially new electronic states are created and these new chemical species are an open door to control the chemistry of simple molecules or to increase our understanding of the molecular dynamics in excited states.

Acknowledgments

This work was supported by the NRF Grant funded by the Korean government (2007-0056343), the International cooperation program (NRF-

2013K2A1A2054518), the Basic Science Research program (NRF-2013R1A1A2061898), the EDISON project (2012M3C1A6035358), and the MICINN project CTQ2012-36184.

* Electronic address: isola@quim.ucm.es

- [1] S. A. Rice, M. Zhao, *Optical Control of Molecular Dynamics*, Wiley-Interscience, **2000**.
- [2] P. W. Brumer, M. Shapiro, *Principles of the Quantum Control of Molecular Processes*, Wiley-Interscience, **2003**.
- [3] M. Wollenhaupt, V. Engel, T. Baumert, *Annu. Rev. Phys. Chem.* **2005**, 56, 25.
- [4] C. Brif, R. Chakrabarti, H. Rabitz, *Adv. Chem. Phys.* **2012**, 148, 1.
- [5] G. A. Worth, *Annu. Rep. Prog. Chem. Sect. C: Phys. Chem.* **2013**, 109, 113.
- [6] A. H. Zewail, *Phys. Today* **1980**, 33, 27.
- [7] H. Rabitz, R. de Vivie-Riedle, K. Kompa, *Science* **2000**, 288, 824.
- [8] B. J. Sussman, D. Townsend, M. Y. Ivanov, A. Stolow, *Science* **2006**, 314, 278.
- [9] J. Kim, H. Tao, J. L. White, V. S. Petrovic, T. J. Martinez, P. H. Bucksbaum, *J. Phys. Chem. A* **2012**, 116, 2758.
- [10] M. E. Corrales, J. González-Vázquez, G. Balerdi, I. R. Sola, R. de Nalda, L. Bañares, *Nat. Chem.* **2014**, 6, 785.
- [11] B. J. Sussman, *Am. J. Phys.* **2011**, 79, 477.
- [12] G. Nuernberger, G. Vogt, T. Briner, G. Gerber, *Phys. Chem. Chem. Phys.* **2007**, 9, 2470.
- [13] D. Townsend, B. J. Sussman, A. Stolow, *J. Phys. Chem. A* **2011**, 115, 357.
- [14] I. R. Sola, J. González-Vázquez, R. de Nalda, L. Bañares, *Phys. Chem. Chem. Phys.* **2015**, 17, 13183.
- [15] P. Agostini, F. Fabre, G. Mainfray, G. Petite, N. K. Rahman, *Phys. Rev. Lett.* **1979**, 42, 1127.
- [16] L. V. Keldysh, *Sov. Phys.-JETP* **1964**, 20, 1307.
- [17] F. H. M. Faisal, *J. Phys. B* **1973**, 6, L89.
- [18] H. R. Reiss, *Phys. Rev. A* **1980**, 22, 1786.
- [19] P. Kruit, J. Kimman, H. G. Muller, M. J. van der Wiel, *Phys. Rev. A* **1983**, 28, 248.
- [20] M. Pont, M. Gavrila, *Phys. Rev. Lett.* **1990**, 65, 2362.
- [21] M. Lewenstein, Ph. Balcau, M. Yu. Ivanov, A. LHuillier, P. B. Corkum, *Phys. Rev. A* **1994**, 49, 2117.
- [22] *Atoms in Intense Laser Fields*; M. Gavrila, Eds.; Academic Press: San Diego, **1992**.
- [23] N. B. Delone, V. P. Krainov, *Multiphoton Processes in Atoms*, 2nd Ed.; Springer: Heidelberg, **2000**.
- [24] *Lectures on Ultrafast Intense Laser Science*, K. Yamanouchi, Eds.; Springer: Heidelberg, **2006**.
- [25] C. J. Joachain, N. J. Kylstra, R. M. Potvliege, *Atoms in Intense Laser Fields*, Cambridge University Press: Cambridge, **2012**.
- [26] J.-M. Yuan, T. F. George, *J. Chem. Phys.* **1978**, 68, 3040.
- [27] A. D. Bandrauk, M. L. Sink, *J. Chem. Phys.* **1981**, 74, 1110.
- [28] A. D. Bandrauk, E. E. Aubanel, J.-M. Gauthier, in *Molecules in Laser Fields*; A. D. Bandrauk, Eds.; Marcel Dekker: New York, **1994**, Chapter 3, pp 109-180.
- [29] E. E. Aubanel, A. D. Bandrauk, *J. Phys. Chem.* **1993**, 97, 12620.
- [30] J. González-Vázquez, L. González, I. R. Sola, J. Santamaria, *J. Chem. Phys.* **2009**, 131, 104302.
- [31] N. Moiseyev, M. Sindelka, L. S. Cederbaum, *J. Phys. B: At., Mol. Opt. Phys.* **2008**, 41, 221001.
- [32] M. Sindelka, N. Moiseyev, L. S. Cederbaum, *J. Phys. B: At., Mol. Opt. Phys.* **2011**, 44, 045603.
- [33] G. J. Halász, M. Sindelka, N. Moiseyev, L. S. Cederbaum, A. Vibok, *J. Phys. Chem. A* **2011**, 116, 2636.
- [34] G. J. Halász, Á. Vibók, M. Sindelka, L. S. Cederbaum, N. Moiseyev, *Chem. Phys.* **2012**, 399, 146.
- [35] P. V. Demekhin, L. S. Cederbaum, *J. Chem. Phys.* **2013**, 139, 154314.
- [36] G. J. Halász, Á. Vibók, N. Moiseyev, L. S. Cederbaum, *Phys. Rev. A* **2013**, 88, 043413.
- [37] G. J. Halász, A. Csehi, Á. Vibók, L. S. Cederbaum, *J. Phys. Chem. A* **2014**, 118, 11908.
- [38] G. J. Halász, Á. Vibók, L. S. Cederbaum, *J. Phys. Chem. Lett.* **2015**, 6, 348.
- [39] A. Natan, M. R. Ware, P. H. Bucksbaum, In *Ultrafast Phenomena XIX*; K. Yamanouchi, S. Cundiff, R. de Vivie-Riedle, M. Kuwata-Gonokami, L. Dimauro, Eds.; Springer: New York, **2015**; Vol. 162, pp. 122-125.
- [40] I. R. Sola, V. S. Malinovsky, *Phys. Rev. A* **2003**, 68, 013412.
- [41] B. Y. Chang, S. Shin, I. R. Sola, *J. Phys. Chem. Lett.* **2015**, 6, 1724.
- [42] B. Y. Chang, S. Shin, I. R. Sola, *J. Chem. Theor. Comput.* **2015**, 11, 4005.
- [43] B. Y. Chang, S. Shin, I. R. Sola, *J. Phys. Chem. A* **2015**, 119, 9091.
- [44] J. S. Melinger, S. R. Gandhi, A. Hariharan, J. X. Tull, W. S. Warren, *Phys. Rev. Lett.* **1992**, 68, 2000.
- [45] Y. B. Band, O. Magnes, *Phys. Rev. A* **1994**, 50, 584.
- [46] J. Cao, C. J. Bardeen, K. R. Wilson, *Phys. Rev. Lett.* **1998**, 80, 1406.
- [47] V. S. Malinovsky, J. L. Krause, *Eur. Phys. J. D* **2001**, 14, 14.
- [48] K. Bergmann, H. Theuer, B. W. Shore, *Rev. Mod. Phys.* **1998**, 70, 1003.
- [49] B. M. Garraway, K.-A. Suominen, *Rep. Prog. Phys.* **1995**, 58, 365.
- [50] N. V. Vitanov, T. Halfmann, B. W. Shore, K. Bergmann, *Annu. Rev. Phys. Chem.* **2001**, 52, 763.
- [51] B. Garraway, K.-A. Suominen, *Phys. Rev. Lett.* **1998**, 80, 932.
- [52] M. Rodriguez, K.-A. Suominen, B. Garraway, *Phys. Rev. A* **2000**, 62, 053413.
- [53] I. R. Sola, J. Santamaria, V. Malinovsky, *Phys. Rev. A* **2000**, 61, 043413.
- [54] I. R. Sola, B. Y. Chang, J. Santamaria, V. Malinovsky, J. Krause, *Phys. Rev. Lett.* **2000**, 85, 4241.
- [55] V. S. Malinovsky, J. Santamaria, I. R. Sola, *J. Phys. Chem. A* **2003**, 107, 8259.
- [56] J. González-Vázquez, I. R. Sola and J. Santamaria, *J. Phys. Chem. A* **2006**, 110, 1586.
- [57] J. J. Bajo, J. González-Vázquez, I. R. Sola, J. Santamaria, M. Richter, P. Marquetand, L. González, *J. Phys. Chem. A* **2011**, 116, 2800.
- [58] K.-A. Suominen, *J. Mod. Opt.* **2014**, 61, 851.
- [59] S. Kallush, Y. Band, *Phys. Rev. A* **2000**, 61, 041401.
- [60] B. Y. Chang, I. R. Sola, V. S. Malinovsky, J. Santamara, *J. Chem. Phys.* **2000**, 113, 4901.

- [61] B. Y. Chang, B. Kim, I. R. Sola, J. Chem. Phys. **2003**, 118, 6270.
- [62] M. Wollenhaupt, D. Liese, A. Prakelt, C. Sarpe-Tudoran, T. Baumert, Chem. Phys. Lett., **2006**, 419, 184.
- [63] M. Wollenhaupt, T. Baumert, J. Photochem. Photobiol. A **2006**, 180, 248.
- [64] T. Bayer, M. Wollenhaupt, T. Baumert, J. Phys. B: At., Mol. Opt. Phys. **2008**, 41, 074007.
- [65] M. Wollenhaupt, T. Bayer, N. V. Vitanov, T. Baumert, Phys. Rev. A: At., Mol., Opt. Phys. **2010**, 81, 053422.
- [66] S. Chelkowski, G. N. Gibson, Phys. Rev. A **1995**, 52, R3417.
- [67] S. Chelkowski, A. D. Bandrauk, Raman Spectrosc. **1997**, 28, 459.
- [68] J. C. Davis, W. S. Warren, J. Chem. Phys. **1999**, 110, 4229.
- [69] F. Legare, S. Chelkowski, A. D. Bandrauk, Chem. Phys. Lett. **2000**, 329, 469.
- [70] B. Y. Chang, I. R. Sola, J. Santamaria, J. Phys. Chem. A **2001**, 105, 8864.
- [71] B. Y. Chang, I. R. Sola, J. Santamaria, Chem. Phys. Lett. **2001**, 341, 373.
- [72] P. H. Bucksbaum, A. Zavriyev, H. B. Muller, D. W. Schumacher, Phys. Rev. Lett. **1990**, 64, 1883.
- [73] A. Zavriyev, P. H. Bucksbaum, H. B. Muller, D. W. Schumacher, Phys. Rev. A **1990**, 42, 5500.
- [74] B. Yang, M. Saeed, L. F. DiMauro, A. Zavriyev, P. H. Bucksbaum, Phys. Rev. A **1991**, 44, R1458.
- [75] S. W. Allendorf, A. Szoke, Phys. Rev. A **1991**, 44, 518.
- [76] G. Jolicard, O. Atabek, Phys. Rev. A **1992**, 46, 5845.
- [77] A. Giusti-Suzor, F. H. Mies, L. F. Dimauro, E. Charron, B. Yang, J. Phys. B: At. Mol. Opt. Phys. **1995**, 28, 309.
- [78] A. Giusti-Suzor, F. H. Mies, Phys. Rev. Lett. **1992**, 68, 3869.
- [79] G. Yao, S. I. Chu, Chem. Phys. Lett. **1992**, 197, 413.
- [80] A. Zavriyev, P. H. Bucksbaum, J. Squier, F. Salane, Phys. Rev. Lett. **1993**, 70, 1077.
- [81] E. E. Aubanel, J. M. Gauthier, A. D. Bandrauk, Phys. Rev. A **1993**, 48, 2145.
- [82] E. E. Aubanel, A. Conjusteau, A. D. Bandrauk, Phys. Rev. A **1993**, 48, R4011.
- [83] B. Y. Chang, B. Kim, I.R. Sola, J. Chem. Phys. **2003**, 118, 6270.
- [84] B. Y. Chang, H. Rabitz, I. R. Sola, Phys. Rev. A **2003**, 68, 031402.
- [85] B. Y. Chang, S. Lee, I. R. Sola, J. Chem. Phys. **2004**, 121, 11118.
- [86] B. Y. Chang, S. Shin, A. Palacios, F. Martin, I. R. Sola, ChemPhysChem **2013**, 14, 1405.
- [87] B. Y. Chang, S. Shin, I. R. Sola, Phys. Rev. A **2010**, 82, 063414.
- [88] I. R. Sola, S. Shin, B.Y. Chang, J. Chem. Phys. **2011**, 134, 104301.
- [89] B. Y. Chang, S. Shin, J. Santamaria, I. R. Sola, J. Chem. Phys. **2011**, 134, 144303.
- [90] B. Y. Chang, S. Shin, J. Santamaria, I. R. Sola, J. Phys. Chem. A **2012**, 116, 2691.
- [91] I. R. Sola, Phys. Rev. A **2004**, 69, 033401.
- [92] B. Y. Chang, S. Lee, I. R. Sola, J. Santamaria, J. Chem. Phys. **2005**, 122, 204316.
- [93] B. Y. Chang, I. R. Sola, J. Chem. Phys. **2005**, 123, 244101.
- [94] B. Y. Chang, I. R. Sola, S. Lee, J. Santamaria, Phys. Rev. A **2006**, 73, 023407.
- [95] B. Y. Chang, S. Lee, I.R. Sola, J. Santamaria, Phys. Rev. A **2006**, 73, 013404.
- [96] B. Y. Chang, S. Lee, I. R. Sola, J. Santamaria, J. Photochem. Photobiol. A **2006**, 180, 241.
- [97] B. Y. Chang, S. Shin, A. Palacios, F. Martin, I. R. Sola, J. Chem. Phys. **2013**, 139, 084306.
- [98] E. Persson, J. Burgdörfer, S. Gräfe, New. J. Phys. **2009**, 11, 105035.
- [99] B. Y. Chang, S. Shin, A. Palacios, F. Martin, I. R. Sola, J. Phys. B: At. Mol. Opt. Phys. **2015**, 48, 043001.
- [100] B. Y. Chang, S. Shin, V. Malinovsky, I. R. Sola, J. Phys. B: At. Mol. Opt. Phys. **2015**, 48, 174005.
- [101] J. González-Vázquez, I. R. Sola, J. Santamaria, V. S. Malinovsky, Chem. Phys. Lett. **2006**, 431, 231.
- [102] J. González-Vázquez, I. R. Sola, J. Santamaria, V. S. Malinovsky, J. Chem. Phys. **2006**, 125, 124315.
- [103] J. González-Vázquez, I.R. Sola, J. Santamaria, V. S. Malinovsky, J. Phys. Chem. A **2007**, 111, 2670.
- [104] M. Falge, V. Engel, M. Lein, P. Vindel-Zandbergen, B. Y. Chang, I. R. Sola, J. Phys. Chem. A **2012**, 116, 11427.
- [105] M. Falge, P. Vindel-Zandbergen, V. Engel, M. Lein, B. Y. Chang, I. R. Sola, J. Phys. B: At. Mol. Opt. Phys. **2014**, 47, 124027.
- [106] I. R. Sola, J. González-Vázquez, V. S. Malinovsky, Phys. Rev. A **2006**, 74, 043418.
- [107] B. J. Sussman, M. Y. Ivanov, A. Stolow, Phys. Rev. A **2005**, 71, 051401.
- [108] H. Choi, W. J. Son, S. Shin, B. Y. Chang, I. R. Sola, J. Chem. Phys. **2008**, 128, 104315.
- [109] B. Y. Chang, H. Choi, S. Shin, I. Sola, J. Modern Opt. **2009**, 56, 811.
- [110] B. Y. Chang, S. Shin, J. Santamaria, I. R. Sola, J. Chem. Phys., **2009**, 130, 124320.
- [111] B. Y. Chang, S. Shin, I. R. Sola, J. Chem. Phys., **2009**, 131, 204314.
- [112] J. Javanainen, J. Eberly, Q. Su, Phys. Rev. A **1988**, 38, 3430.
- [113] Q. Su, J. Eberly, Phys. Rev. A **1991**, 44, 5997.
- [114] K. C. Kulander, F. H. Mies, K. J. Schafer, Phys. Rev. A **1996**, 53, 2562.
- [115] A. D. Bandrauk, H. Kono, in Advances in Multi-Photon Processes and Spectroscopy; S.H. Lin, A. Villaeys, Y. Fujimura, Eds.; World Scientific: Singapore, **2003** vol. 15, pp 149-214.
- [116] H. Kono, Y. Sato, M. Kanno, K. Nakai, T. Kato, Bull. Chem. Soc. Jpn. **2006**, 79, 196.
- [117] T. Zuo, A. D. Bandrauk, Phys. Rev. A **1995**, 52, R2511.
- [118] H. Niikura, D. M. Villeneuve, P. B. Corkum, Phys. Rev. Lett. **2004**, 92, 133002.
- [119] G. Balerdi, M. E. Corrales, G. Gitzinger, J. González-Vázquez, I. R. Sola, V. Loriot, R. de Nalda, L. Bañares, EPJ Web Conf. **2013**, 41, 02035.
- [120] S. Meyer, C. Meier, V. Engel, J. Chem. Phys. **1998**, 108, 7631.
- [121] P. E. Maslen, J. Faeder, R. Parson, Chem. Phys. Lett. **1996**, 263, 63.
- [122] M. Lein, M. Erdmann, V. Engel, J. Chem. Phys. **2009**, 113, 3609.